

Measure Estimation in the Barycentric Coding Model

Matthew Werenski* Ruijie Jiang[†] Abiy Tasissa[‡]

Shuchin Aeron[†] James M. Murphy[‡]

January 31, 2022

Abstract

This paper considers the problem of measure estimation under the *barycentric coding model (BCM)*, in which an unknown measure is assumed to belong to the set of Wasserstein-2 barycenters of a finite set of known measures. Estimating a measure under this model is equivalent to estimating the unknown barycentric coordinates. We provide novel geometrical, statistical, and computational insights for measure estimation under the BCM, consisting of three main results. Our first main result leverages the Riemannian geometry of Wasserstein-2 space to provide a *procedure for recovering the barycentric coordinates as the solution to a quadratic optimization problem* assuming access to the true reference measures. The essential geometric insight is that the parameters of this quadratic problem are determined by inner products between the optimal displacement maps from the given measure to the reference measures defining the BCM. Our second main result then establishes an *algorithm for solving for the coordinates in the BCM when all the measures are observed empirically via i.i.d. samples*. We prove precise *rates of convergence* for this algorithm—determined by the smoothness of the underlying measures and their dimensionality—thereby guaranteeing its statistical consistency. Finally, we demonstrate the utility of the BCM and associated estimation procedures in three application areas: (i) *covariance estimation* for Gaussian measures; (ii) *image processing*; and (iii) *natural language processing*.

1 Introduction

A number of recent machine learning applications including computer vision [42, 9], domain adaptation [32, 40], natural language processing (NLP) [44, 16, 47], and unsupervised segmentation of multivariate time series data [12] have shown the utility of representing and modeling high-dimensional data as probability distributions. The essential insight

*Department of Computer Science, Tufts University, Medford, MA 02155, USA (matthew.werenski@tufts.edu)

[†]Department of Electrical and Computer Engineering, Tufts University, Medford, MA 02155, USA (ruijie.jiang@tufts.edu, shuchin@ece.tufts.edu)

[‡]Department of Mathematics, Tufts University, Medford, MA 02155, USA (abiy.tasissa@tufts.edu, jm.murphy@tufts.edu)

in these applications is to utilize the Riemannian geometry of the space of probability distributions induced by the Wasserstein-2 metric and the Wasserstein-2 barycenters as alternatives to the Euclidean distance and linear combinations, respectively.

In this context, the methods that use Wasserstein barycenters for data modeling and inference involve solving two core problems which we term the *synthesis problem* and *analysis problem*. To be precise, let $\mathcal{P}_{2,\text{ac}}(\mathbb{R}^d)$ denote the space of absolutely continuous distributions on \mathbb{R}^d with finite second moment. For $\mu, \nu \in \mathcal{P}_{2,\text{ac}}(\mathbb{R}^d)$,

$$W_2^2(\mu, \nu) \triangleq \min_{T \# \mu = \nu} \int_{\mathbb{R}^d} \|T(x) - x\|_2^2 d\mu(x) \quad (1)$$

defines the *Wasserstein-2 metric* where the minimum is over all measurable maps $T : \mathbb{R}^d \rightarrow \mathbb{R}^d$ and the *pushforward* $T \# \mu = \nu$ is such that for all Borel sets B we have $\nu[B] = \mu[T^{-1}(B)]$ [46, 41]. Under the assumption $\mu, \nu \in \mathcal{P}_{2,\text{ac}}(\mathbb{R}^d)$, unique minimizing T are known to exist and the resulting W_2 distance is finite [46]. We refer to the space $\mathcal{P}_{2,\text{ac}}(\mathbb{R}^d)$ equipped with the metric W_2 as the *Wasserstein-2 space*, denoted \mathcal{W}_2 .

Let $\Delta^p = \{\lambda = (\lambda_1, \dots, \lambda_p) \in \mathbb{R}^p : \lambda_i \geq 0, \sum_{i=1}^p \lambda_i = 1\}$ and let $\{\mu_i\}_{i=1}^p$ be known *reference measures*. The W_2 *barycenter* for coordinates $\lambda \in \Delta^p$ with respect to $\{\mu_i\}_{i=1}^p$ is defined as

$$\nu_\lambda \triangleq \arg \min_{\nu \in \mathcal{P}_{2,\text{ac}}(\mathbb{R}^d)} \frac{1}{2} \sum_{i=1}^p \lambda_i W_2^2(\nu, \mu_i) \quad (2)$$

The measure ν_λ is an advection of $\{\mu_i\}_{i=1}^p$ and blends their geometric features; it may be thought of as a “displacement interpolation” [30, 46]. In contrast, the linear mixture $\sum_{i=1}^p \lambda_i \mu_i$ simply sets λ_i to be the rate we draw samples from μ_i . Figure 1 demonstrates the important difference between linear mixture models and Wasserstein barycenters on Gaussian distributions: the linear mixture is a standard Gaussian mixture model [33], while the Wasserstein barycenter is itself Gaussian. The important take away is that Wasserstein barycenters offer a more geometrically meaningful interpolation between measures compared to mixtures, and as indicated above have been successfully exploited in a number of applications.

Now, let $\text{Bary}(\{\mu_i\}_{i=1}^p) \triangleq \{\nu_\lambda : \lambda \in \Delta^p\}$ denote the set of all of possible barycenters of $\{\mu_i\}_{i=1}^p$. The *synthesis problem* (2) seeks to combine the reference measures $\{\mu_i\}_{i=1}^p$ in a notion of weighted average, with relative contributions determined by λ . This problem is well-studied [30, 1, 27] and known to have a unique solution under mild assumptions on the $\{\mu_i\}_{i=1}^p$. Moreover, there exist fast algorithms for computing or approximating ν_λ when samples from the $\{\mu_i\}_{i=1}^p$ are available [39, 18, 10, 15, 48], which have spurred the application of Wasserstein barycenters to machine learning problems.

In this paper, our focus is on the less well-studied *analysis problem*: given μ_0 and reference measures $\{\mu_i\}_{i=1}^p$, solve

$$\arg \min_{\lambda \in \Delta^p} W_2^2(\mu_0, \nu_\lambda). \quad (3)$$

Instead of *combining* the measures $\{\mu_i\}_{i=1}^p$ according to the weights $\lambda \in \Delta^p$ as in (2), the analysis problem (3) *decomposes* a given measure μ_0 into its optimal representation in the set $\text{Bary}(\{\mu_i\}_{i=1}^p)$ as parametrized by the learned barycentric coordinates $\lambda \in \Delta^p$. If the measure $\mu_0 \in \text{Bary}(\{\mu_i\}_{i=1}^p)$, then $\min_{\lambda \in \Delta^p} W_2^2(\mu_0, \nu_\lambda) = 0$ and solving (3) is equivalent to learning the barycentric coordinates $\lambda \in \Delta^p$ such that $\nu_\lambda = \mu_0$. We refer to this general

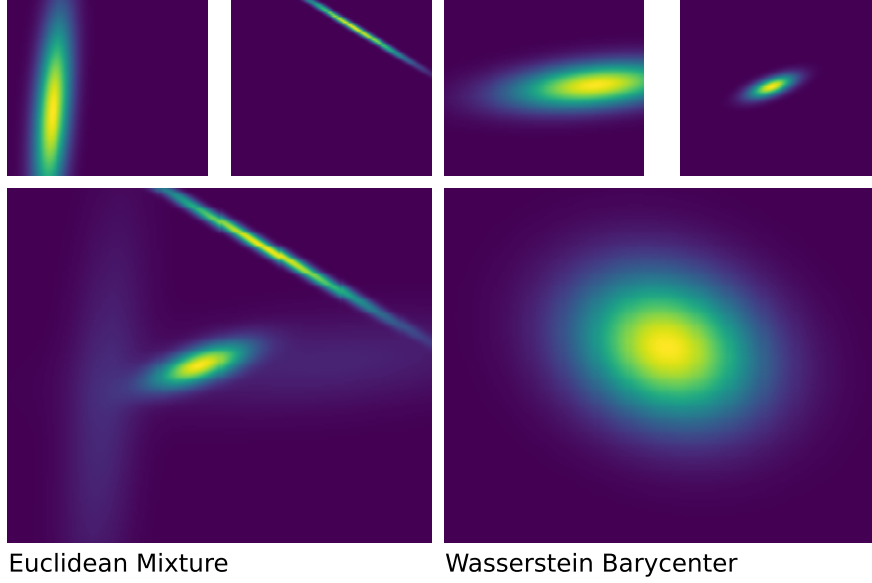


Figure 1: *Top four*: reference Gaussians. *Bottom left*: linear mixture with $\lambda = (\frac{1}{4}, \frac{1}{4}, \frac{1}{4}, \frac{1}{4})$. *Bottom right*: Wasserstein barycenter with same λ . (Intensities adjusted to show detail.)

model of parameterizing measures $\mu_0 \in \text{Bary}(\{\mu_i\}_{i=1}^p)$ through the associated coordinates $\lambda \in \Delta^p$ as the *barycentric coding model* (BCM).

Main Contributions: This paper addresses the analysis problem (3) as a measure estimation problem under the BCM. For this general problem, we make the following geometrical, statistical, and computational contributions:

- (1) When all the measures are directly observed, Theorem 1 provides a *geometric* characterization of the solution to (3) as corresponding to a solution to a quadratic program. Our analysis leverages the Riemannian geometry of \mathcal{W}_2 space and establishes that the quadratic program is determined by the angles between the optimal displacement maps between the measures. When specialized to the case of Gaussian measures, Corollary 1 provides a closed-form characterization of the solution to the analysis problem.
- (2) When the measures are indirectly observed via i.i.d. samples, we provide an algorithm for estimating the barycentric coordinates λ of a given measure with respect to the reference measures. Theorem 2 gives precise rates of convergence of the angles between the optimal displacement map by a computationally tractable estimator that exploits entropic regularization, thereby establishing the statistical consistency of our approach in Corollary 2.
- (3) We showcase the utility of the BCM and the proposed algorithm on several data analysis problems: covariance estimation for Gaussian measures; image inpainting and denoising; and document classification from limited labeled data. We show that the BCM provides a simple yet effective approach that outperforms competing methods in the regimes considered.¹

¹Code to reproduce results is publicly available on MW's github.

1.1 Related Work

The synthesis problem (2) is well-studied. [1] propose W_2 barycenters for a finite set of reference measures $\{\mu_i\}_{i=1}^p$ and prove their existence and uniqueness in a very general setting. [8] extend this to barycenters constructed from infinitely many reference measures. Statistical rates of estimation in the setting of i.i.d. samples from the measures $\{\mu_i\}_{i=1}^p$ are established in [27]. Building on fundamental advances in estimating transport maps between measures using entropic regularization [17], fast estimation methods for solving the synthesis problem have been developed for entropically regularized barycenters [18]. Approaches to computing a barycenter based on alternating direction of multipliers on the dual problem [48] and parallelization schemes [15] have also been considered.

The literature on the analysis problem (3) is much sparser. To the best of our knowledge, our geometrical characterization of solutions to the analysis problem (Theorem 1) and sample complexity results for estimating the optimal coordinates λ (Theorem 2, Corollary 2) are the first of their kind. Note that our approach extends [9, 42]—which consider measure estimation under the BCM but only for measures with finite support—in three fundamental ways. First, we enable the application of the BCM to absolutely continuous measures. Second, we prove precise theoretical characterizations of the solutions to (3). Third, we avoid the expensive procedure of differentiating through an iterative algorithm as required in [9] and instead provide the direct Algorithm 1 that enjoys statistical consistency (Corollary 2). At the level of technical analysis, our Theorem 1 relies on an alternative characterization of W_2 barycenters that leverages known conditions under which Karcher means are guaranteed to be W_2 barycenters [35].

For the special case when all the measures are zero-mean Gaussians, the *synthesis* problem is again well-studied, with a fixed-point algorithm for computing the barycenter given in [4] that is shown to have a linear convergence rate in [13, 3]. The corresponding *analysis* problem for the specific case of Gaussian measures has only been recently studied in [34] but limited to the case when $p = 2$. When specialized to this case, our results extend the model considered in [34] to the $p \geq 3$ case and characterize solutions to barycenter parametrized covariance estimation.

In Section 4, we use the proposed BCM framework to model and address several problems in image processing and natural language processing. In this context our work is related to a long lineage of methods in signal processing and machine learning that use coefficients in a basis or a dictionary for data modeling and processing [29, 20, 45]. Our approach of representing a general measure in terms of its barycentric coordinates with respect to a fixed set of reference measures is a novel approach in this tradition, and our results in Section 4 suggest its utility for data modeled as probability measures.

2 Convex Optimization for the Analysis Problem

To solve the analysis problem (3), we propose to solve a convex optimization problem based on an alternative characterization of W_2 -barycenters as minimizers of a certain functional. We leverage this alternative characterization to show in Theorem 1 that, under mild assumptions on $\{\mu_i\}_{i=1}^p$, one can use the optimal value of a convex program to both check if $\mu_0 \in \text{Bary}(\{\mu_i\}_{i=1}^p)$ and if so, recover its barycentric coordinate. Before proceeding, we must introduce some background on the Riemannian geometry of the \mathcal{W}_2 space. The

geodesic curve from ν_0 to ν_1 in \mathcal{W}_2 is given by $[\nu_t]_{t=0}^1$ where $\nu_t = (tT + (1-t)\text{Id})\#\nu_0$ where T is the optimal map from ν_0 to ν_1 in (1) [41]. These facts together with Brenier's Theorem (see Supplementary Material Section 1) motivate the definition of the tangent space at ν :

$$T_\nu \mathcal{P}_{2,\text{ac}}(\mathbb{R}^d) \triangleq \overline{\{\beta(\nabla\varphi - \text{Id}) : \beta > 0, \varphi \in C_c^\infty(\mathbb{R}^d), \varphi \text{ convex}\}},$$

where the closure is in $L^2(\nu)$ [5]. For $u, v \in T_\nu \mathcal{P}_{2,\text{ac}}(\mathbb{R}^d)$, the inner product is defined by $\langle u, v \rangle_\nu \triangleq \int_{\mathbb{R}^d} \langle u(x), v(x) \rangle d\nu(x)$, which also gives the standard norm of $u \in T_\nu \mathcal{P}_{2,\text{ac}}(\mathbb{R}^d)$, $\|u\|_\nu \triangleq \sqrt{\langle u, u \rangle_\nu}$.

2.1 Alternative Characterization of Barycenters

Given the reference measures $\{\mu_i\}_{i=1}^p$ and barycentric coordinates $\lambda \in \Delta^p$, the *variance functional* is $G_\lambda : \mathcal{P}_{2,\text{ac}}(\mathbb{R}^d) \rightarrow \mathbb{R}$ defined by

$$G_\lambda(\nu) \triangleq \sum_{i=1}^p \frac{\lambda_i}{2} W_2^2(\nu, \mu_i),$$

so that the barycenter for $\{\mu_i\}_{i=1}^p$ and $\lambda \in \Delta^p$ is

$$\nu_\lambda = \arg \min_{\nu \in \mathcal{P}_{2,\text{ac}}(\mathbb{R}^d)} G_\lambda(\nu).$$

In many unconstrained optimization problems, the most direct way of checking if a point is optimal is to use first-order optimality conditions: compute the gradient at the point and check if it is zero. Without further assumptions this is a necessary, but not sufficient, condition for optimality. Applying this to a general variance functional, one arrives at the definition of a *Karcher mean* [26].

Definition 1. Let (X, ρ) be a metric space furnished with a tangent space at every $x \in X$. For a collection of points $\{x_i\}_{i=1}^p \subset X$ and coordinates $\lambda \in \Delta^p$, a point $y \in X$ is said to be a *Karcher mean* of the set for λ if $G_\lambda = \sum_{i=1}^p \lambda_i \rho^2(\cdot, x_i)$ is differentiable at y and $\|\nabla G_\lambda(y)\|_y = 0$ where $\nabla G_\lambda(y)$ is understood as an element of the tangent space at y .

Any barycenter y is a global minimizer of G_λ . Using first order optimality conditions, this implies $\|\nabla G_\lambda(y)\|_y = 0$, and therefore y must be a Karcher mean. Special care must be made to ensure that being a Karcher mean is sufficient to be a barycenter. When it is sufficient, it immediately gives an alternative test for y to be a barycenter for λ : simply check if $\|\nabla G_\lambda(y)\|_y = 0$.

An example of a Karcher mean which is not a barycenter is given in the Supplementary Material Section 7. To ensure that being a Karcher mean is sufficient to be a barycenter we require the following assumptions:

A1: The measures μ_0, \dots, μ_p are absolutely continuous and supported on either all of \mathbb{R}^d or a bounded open convex subset. Call this shared support set Ω .

A2: The measures μ_0, \dots, μ_p have respective densities g_0, \dots, g_p which are bounded above and g_1, \dots, g_p are strictly positive on Ω .

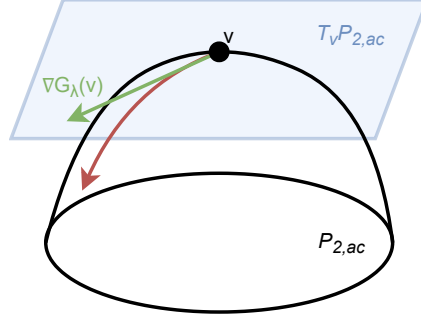


Figure 2: Visualization of the tangent space $T_\nu \mathcal{P}_{2,ac}(\mathbb{R}^d)$ and ∇G_λ . The red arc is the path along which G_λ is maximized, starting at ν and the green arrow points in that direction in the tangent space at ν .

A3: If $\Omega = \mathbb{R}^d$ then g_0, \dots, g_p are locally Hölder continuous. Otherwise g_0, \dots, g_p are bounded away from zero on Ω .

Under these assumptions if μ_0 is a Karcher mean with coordinates λ , then $\mu_0 = \nu_\lambda$ [35]; see the Supplementary Material Section 1 for a precise statement.

This characterization of barycenters can be much easier to work with and the assumptions required are mild in practice. To accompany the notion of a Karcher mean, the *Fréchet derivative* [21] of the variance functional G_λ is given by

$$\nabla G_\lambda(\nu) = - \sum_{i=1}^p \lambda_i (T_i - \text{Id}), \quad (4)$$

where T_i is the optimal map from ν to μ_i as in (1) [5, 35].

We now have all the tools to begin building up to Theorem 1. The first step is to derive a formula for $\|\nabla G_\lambda(\mu_0)\|_{\mu_0}^2$ in terms of λ and show its convexity.

Proposition 1. *Let $\{\mu_i\}_{i=0}^p \subset \mathcal{P}_{2,ac}(\mathbb{R}^d)$. Then $\|\nabla G_\lambda(\mu_0)\|_{\mu_0}^2 = \lambda^T A \lambda$ where $A \in \mathbb{R}^{p \times p}$ is given by*

$$A_{ij} = \int_{\mathbb{R}^d} \langle T_i(x) - \text{Id}(x), T_j(x) - \text{Id}(x) \rangle d\mu_0(x) \quad (5)$$

and T_i is the optimal map from μ_0 to μ_i as in (1). Furthermore, this is a convex function in λ .

The proof is given in the Supplementary Material Section 2.1. The expression $T_i(x) - \text{Id}(x)$ is the displacement of the point x when being transported from μ_0 to μ_i . Under this interpretation, $\langle T_i(x) - \text{Id}, T_j(x) - \text{Id} \rangle$ can be thought of as the angle between the displacement associated to the optimal transport map between μ_0 to μ_i with that of μ_0 to μ_j . Integrating this quantity with respect to μ_0 therefore quantifies the average angle between displacements and if the optimal displacement maps move in similar directions.

We now use this functional form as part of a convex program and show that it can be used to check if a μ_0 is a Karcher mean. Our first main result ties Propositions 1 to the conditions for equivalence between barycenters and Karcher means.

Theorem 1. *Let $\{\mu_i\}_{i=0}^p$ satisfy **A1-A3**. Then $\mu_0 \in \text{Bary}(\{\mu_i\}_{i=1}^p)$ if and only if*

$$\min_{\lambda \in \Delta^p} \lambda^T A \lambda = 0$$

where $A \in \mathbb{R}^{p \times p}$ is given by (5). Furthermore, if the minimum value is 0 and λ_* is an optimal argument, then $\mu_0 = \nu_{\lambda_*}$.

The proof is given in the Supplementary Material Section 2.3. Theorem 1 gives a geometric characterization of the solution to (3) which relies on the evaluation of inner-products in the tangent space $T_{\mu_0} \mathcal{P}_{2,\text{ac}}(\mathbb{R}^d)$ (noting that $A_{ij} = \langle T_i - \text{Id}, T_j - \text{Id} \rangle_{\mu_0}$) and solving a constrained quadratic program. Furthermore, this result suggests a method for finding an approximator of the μ_0 in the set of barycenters: simply minimize the objective and use λ_* , even if the minimum value is not zero.

Note that if A has rank less than $p - 1$ there may be multiple minimizers which correspond to redundancies in the set $\text{Bary}(\{\mu_i\}_{i=1}^p)$; see Supplementary Material Section 6.

2.2 Theorem 1 For Gaussians

In the Gaussian case there are formulas for both the optimal maps and the integration involved in A_{ij} . Let \mathbb{S}_{++}^d denote the set of symmetric positive definite $d \times d$ matrices. Let $\mu_i = \mathcal{N}(0, S_i)$ with $S_i \in \mathbb{S}_{++}^d$ for $i = 0, \dots, p$. Then the optimal map from μ_0 to μ_i is given by $T_i(x) = C_i x$ where

$$C_i = S_0^{-1/2} \left(S_0^{1/2} S_i S_0^{1/2} \right)^{1/2} S_0^{-1/2} \quad (6)$$

[1]. Furthermore, **A1-A3** are satisfied for non-degenerate Gaussians. Combining Theorem 1 with (6) gives the following.

Corollary 1. *For $i = 1, \dots, p$, let $\mu_i = \mathcal{N}(0, S_i)$ with $S_i \in \mathbb{S}_{++}^d$. Then μ_0 is a barycenter if and only if $\mu_0 = \mathcal{N}(0, S_0)$ for some $S_0 \in \mathbb{S}_{++}^d$, and the convex program of Theorem 1 has minimum value 0, where the matrix A is given by $A_{ij} = \text{Tr}((C_i - I)(C_j - I)S_0)$. Furthermore, if the minimum value is zero and λ_* is a optimal argument, then $\mu_0 = \nu_{\lambda_*}$.*

The proof is deferred to the Supplementary Material Section 2.3. We note that in the Gaussian case, one can use $\|\nabla G_\lambda(\mu_0)\|_{\mu_0}$ to upper bound $W_2(\mu_0, \nu_\lambda)$ [13, 3]. This further justifies the choice of optimizing $\|\nabla G_\lambda(\mu_0)\|_{\mu_0}^2$, since it can be seen as a convex, sharp upper bound on the distance to the set of barycenters.

3 Finite Sample Analysis and Rates of Convergence

The results of the previous section are all reliant upon having exact knowledge of both the underlying measure μ_0 as well as the optimal transport maps T_i . In practice, outside of specific parametric families (e.g., Gaussians), it is rare that one will have either of these available to them.

Much more common is the setting where the μ_i are accessed through i.i.d. sampling. In this setting we need to estimate the maps T_i , as well as μ_0 and use these estimates to compute an \hat{A} whose entries are $\hat{A}_{ij} = \langle \hat{T}_i - \text{Id}, \hat{T}_j - \text{Id} \rangle_{\hat{\mu}_0}$, where \hat{T}_i and $\hat{\mu}_0$ are our estimates of the transport maps and μ_0 respectively. The quality of the estimate \hat{A} will depend on the approximations used above, and ideally these would be accompanied by performance guarantees.

3.1 The Entropic Map Estimate

Let $X_1, \dots, X_n \sim \mu_0$ and $Y_1, \dots, Y_n \sim \mu_1$ be i.i.d. samples. In [37] the authors propose using the *entropic map* to estimate the transport maps. For $\epsilon > 0$, this map is defined by

$$\hat{T}_\epsilon(x) \triangleq \frac{\frac{1}{n} \sum_{i=1}^n Y_i \exp \left(\frac{1}{\epsilon} (g_\epsilon(Y_i) - \frac{1}{2} \|x - Y_i\|_2^2) \right)}{\frac{1}{n} \sum_{i=1}^n \exp \left(\frac{1}{\epsilon} (g_\epsilon(Y_i) - \frac{1}{2} \|x - Y_i\|_2^2) \right)} \quad (7)$$

where g_ϵ is defined to be the optimal variable in the dual entropic optimal transport problem on the samples. See the Supplementary Material 1.1 for details on g_ϵ and important properties of \hat{T}_ϵ . Practically, the calculation of g_ϵ has been well studied and there exists fast algorithms for its computation [36]. The estimate has also been shown to converge (with rates) to the optimal map in $L_2(\mu_0)$ under the appropriate technical conditions.

Algorithm 1 Estimate λ

Input: i.i.d. samples $\{X_1, \dots, X_{2n}\} \sim \mu_0, \{\{Y_1^i, \dots, Y_n^i\} \sim \mu_i : i = 1, \dots, p\}$, regularization parameter $\epsilon > 0$.

for $i = 1, \dots, p$ **do**

Set $M^i \in \mathbb{R}^{n \times n}$ with $M_{jk}^i = \frac{1}{2} \|X_j - Y_k^i\|_2^2$.

Solve for g^i as the optimal g in

$$\begin{aligned} \max_{f, g \in \mathbb{R}^n} & \frac{1}{n} \sum_{j=1}^n f_j + \frac{1}{n} \sum_{k=1}^n g_k \\ & - \frac{\epsilon}{n^2} \sum_{j,k} \exp((f_j + g_k - M_{jk}^i)/\epsilon) \end{aligned}$$

Define \hat{T}_i through 7 with $g_\epsilon = g_i$ and $\{Y_1^i, \dots, Y_n^i\}$.

end for

Set $\hat{A} \in \mathbb{R}^{p \times p}$ to be the matrix with entries

$$\hat{A}_{ij} = \frac{1}{n} \sum_{k=n+1}^{2n} \langle \hat{T}_i(X_k) - X_k, \hat{T}_j(X_k) - X_k \rangle$$

Return $\hat{\lambda} = \arg \min_{\lambda \in \Delta^p} \lambda^T \hat{A} \lambda$.

To accompany this we also have the following result, stated informally below. In this result $a \lesssim b$ means that there exists a constant $C > 0$ such that $a \leq Cb$. We allow this constant C to depend on the size of the support of the measures, upper and lower bounds on their densities, and the regularity properties of the optimal maps T_i, T_j , but it is importantly independent of the sample size n .

Theorem 2. (Informal) Let $i, j \in \{1, \dots, p\}$ and suppose that μ_i, μ_j, μ_0 are supported on bounded domains and that the maps T_i and T_j are sufficiently regular. Let $X_1, \dots, X_{2n} \sim$

$\mu_0, Y_1, \dots, Y_n \sim \mu_i, Z_1, \dots, Z_n \sim \mu_j$. For an appropriately chosen ϵ , let \hat{T}_i and \hat{T}_j be the entropic maps computed using $\{X_i\}_{i=1}^n, \{Y_i\}_{i=1}^n, \{Z_i\}_{i=1}^n$. Then we have

$$\begin{aligned} \mathbb{E} \left[\left\| A_{ij} - \frac{1}{n} \sum_{k=n+1}^{2n} \langle \hat{T}_i(X_k) - X_k, \hat{T}_j(X_k) - X_k \rangle \right\| \right] \\ \lesssim \frac{1}{\sqrt{n}} + n^{-\frac{\alpha+1}{4(d'+\alpha+1)}} \sqrt{\log n} \end{aligned} \quad (8)$$

where $d' = \lceil d/2 \rceil$, and $\alpha \leq 3$ depends on the regularity of optimal maps.

A precise statement and proof of this theorem is given in the Supplementary Material Section 2.4. Theorem 2 tells us that in expectation, by using the entropic map we can accurately approximate the entries of the matrix A_{ij} , and do so in a numerically feasible way. We chose the entropic map as it is computationally tractable and has competitive convergence rates when compared to the intractable but optimal estimator of [25]. We expect similar analysis holds for other recently proposed estimators [19, 23] under different assumptions.

Theorem 2 can be combined with a matrix perturbation analysis to demonstrate the consistency of the estimated barycentric coordinates $\hat{\lambda}$ from Algorithm 1 for the true ones λ_* when $\mu_0 \in \text{Bary}(\{\mu_i\}_{i=1}^p)$, that is when $\lambda_*^T A \lambda_* = 0$. This is stated more precisely as follows.

Corollary 2. *Let $\hat{\lambda}$ be the random estimate obtained from Algorithm 1. Suppose that A has an eigenvalue of 0 with multiplicity 1 and that $\lambda_* \in \Delta^p$ realizes $\lambda_*^T A \lambda_* = 0$. Then under the assumptions of Theorem 2,*

$$\mathbb{E}[\|\hat{\lambda} - \lambda_*\|_2^2] \lesssim \frac{1}{\sqrt{n}} + n^{-\frac{\alpha+1}{4(d'+\alpha+1)}} \sqrt{\log n}.$$

The proof is deferred to the Supplementary Material Section 2.5. Note that the implicit constant in the inequality of Corollary 2 depends on p in addition to the dependencies of listed above. Corollary 2 ensures that in the large sample limit, the entropic regularization parameter may be chosen to guarantee precise estimation of the true barycentric coordinates. Note that the rate of convergence in Corollary 2 depends crucially on the smoothness of the transport maps between the reference measures (α) and the dimensionality of the space in which they are supported (d').

In the next section we illustrate the utility of the BCM and propose novel approaches based on Theorem 1 and Algorithm 1 for several applications.

4 Applications

4.1 Barycenter Parameterized Covariance Estimation

Extending the set-up in [34], we first consider the case where $\mu_i = \mathcal{N}(0, S_i), S_i \in \mathbb{S}_{++}^d$ for $i = 0, \dots, p$. We will use S_i both as a matrix and to refer to μ_i ; similarly, let S_λ denote ν_λ . Let $\{x_i\}_{i=1}^n$ be i.i.d. samples with empirical covariance \hat{S} . In this setting, we can use the formulas laid out in Corollary 1.

For comparison, we also consider maximum likelihood estimation (MLE) for the parameter λ in the BCM. Let P_λ denote the probability density function of S_λ . The MLE is $\arg \max_{\lambda \in \Delta^p} \prod_{i=1}^n P_\lambda(x_i)$, which is equivalent to minimizing the KL-divergence $D_{KL}(\hat{S}, S_\lambda)$. However, this problem may be non-convex and difficult to optimize. We solve it numerically using auto-differentiation [6] and use the coordinates recovered by this method, which may not be the true MLE.

Experimental Setup: We consider the problem of estimating the covariance matrix S_0 from i.i.d. samples $\{x_i\}_{i=1}^n \sim \mathcal{N}(0, S_0)$ when S_0 is known to be a barycenter of S_1, \dots, S_p . To do so we use the following procedure:

1. **Choose λ and $\{S_i\}_{i=1}^p$:** Select $\lambda \in \Delta^p$ and the reference measures $\{S_i\}_{i=1}^p$ either by hand or at random.
2. **Generate S_λ :** Using Algorithm 1 of [13], find the true barycenter, S_λ .
3. **Sample:** Sample $\{x_i\}_{i=1}^n$ i.i.d. from $\mathcal{N}(0, S_\lambda)$. Compute the empirical covariance $\hat{S} = \frac{1}{n} \sum_{i=1}^n x_i x_i^T$.
4. **Estimate $\hat{\lambda}$:** Perform the optimization in Corollary 1, or use MLE with $S_0 = \hat{S}$ to recover an estimate $\hat{\lambda}$.
5. **Compute $S_{\hat{\lambda}}$:** Again using Algorithm 1 of [13] find $S_{\hat{\lambda}}$ and use that as the estimate of S_λ .

The results are in Figure 3. These show that using our approach (denoted *gradient norm*) we can estimate the underlying covariance matrix much more accurately than the empirical covariance. Our optimization is competitive with the auto-differentiation approach to MLE, while being significantly more stable and much faster (computing all the estimates $\hat{\lambda}$ to generate Figure 3 takes our method only 0.7034 seconds compared to over 4 hours for MLE²). Further details are in the Supplementary Material Section 3.

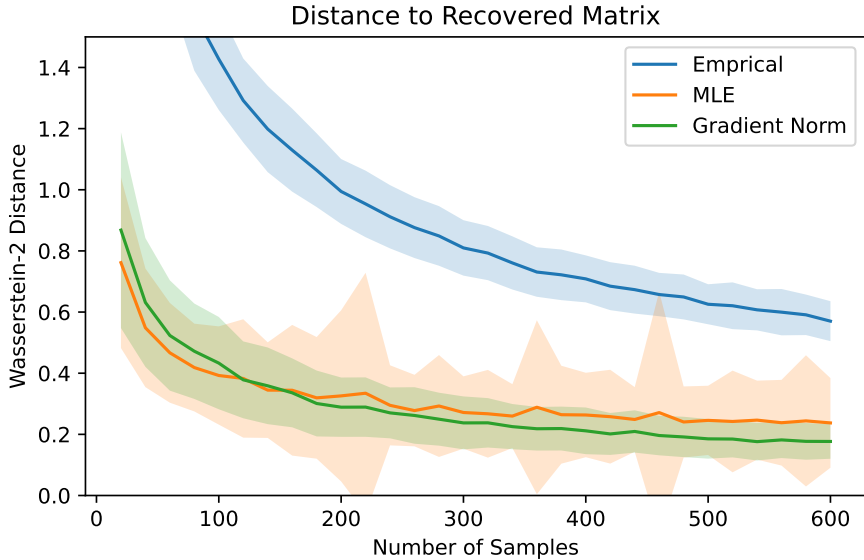


Figure 3: W_2 between true covariance and estimates. We set $p = 6, d = 10$, $\lambda \sim \text{Unif}(\Delta^p)$, and $\mu_i \sim \text{Wish}(I_d) + 0.5I_d$ with results averaged over 250 trials, and 1 standard deviation shaded.

²All reported times are obtained using 20 Intel Xeon CPU E5-2660 V4 cores at 2.00 GHz.

We now consider applications where it is necessary to directly estimate the optimal transport map from samples (unlike the previous case where we estimate it via sample-covariance estimators) and between measures with non-uniform weights on the observed support. To that end, we first modify Algorithm 1 for practical purposes.

4.2 Adapting Algorithm 1 for Applications

In practice, Algorithm 1 has a few mild requirements: that we use the same number of samples for each reference measure; that the weight on each sample is the same; and access to an extra set of points for evaluating the inner products. Algorithm 2 relaxes these requirements and is in terms of matrix-vector operations, making it suitable for practical implementation. Note that Algorithms 1 and 2 are closely related, as both are barycentric projections of the optimal entropic maps [37].

Algorithm 2 Estimate λ on Point Clouds

Input: PMFs $p \in \mathbb{R}^{n_0}$, $q^i \in \mathbb{R}^{n_i}$, support matrices $X \in \mathbb{R}^{n_0 \times d}$, $Y^i \in \mathbb{R}^{n_i \times d}$, regularization parameter $\epsilon > 0$.

for $i = 1, \dots, p$ **do**

Set $M^i \in \mathbb{R}^{n_0 \times n_i}$ with $M_{jk}^i = \|X_j - Y_k^i\|_2^2$

Solve for the entropic assignment matrix π^i as the optimal matrix in

$$\min_{\substack{\pi \in \mathbb{R}_+^{n_0 \times n_i} \\ \pi \mathbf{1} = p \\ \pi^T \mathbf{1} = q^i}} \sum_{j=1}^{n_0} \sum_{k=1}^{n_i} M_{jk}^i \pi_{jk} + \epsilon \pi_{jk} \log \pi_{jk}$$

Compute the approximate transport matrix $\hat{T}_i \in \mathbb{R}^{n_0 \times d}$

$$\hat{T}_i = \text{diag}(1/p) \pi^i Y^i$$

end for

Set $\hat{A} \in \mathbb{R}^{p \times p}$ to be the matrix with entries

$$\hat{A}_{ij} = \text{Tr}(\text{diag}(p)(T^i - X)(T^j - X)^T)$$

Return $\hat{\lambda} = \arg \min_{\lambda \in \Delta^p} \lambda^T \hat{A} \lambda$.

4.3 Image Inpainting and Denoising

We consider the problem of recovering an image in the presence of corruption, interpreting the image as a probability measure. We consider two specific models of corruption: **a.** additive *noise* and **b.** *occlusion* of a portion of the image. Our experimental procedure for both of these problems is outlined below taking as experimental data the MNIST dataset of 28×28 pixel images of hand-written digits [28]. Additional details are in Supplementary Material Section 4. Note that after normalization, these can be treated as measures supported on a 28×28 grid.

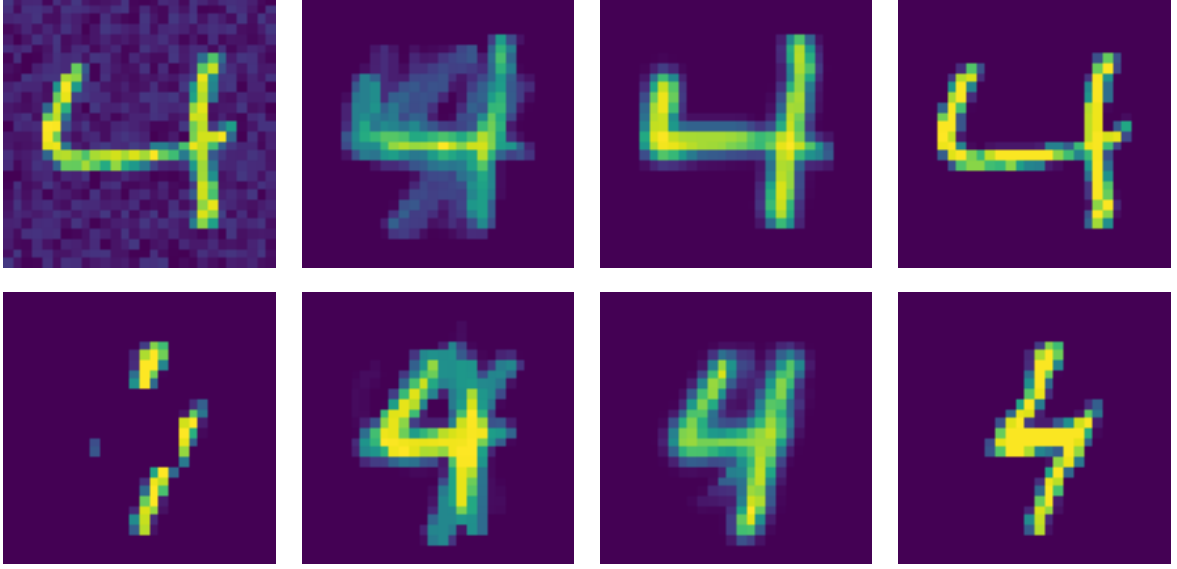


Figure 4: *Left to right*: corrupted image; recovery by linear projection; recovery using $\hat{\lambda}$ from Algorithm 2; original image. *Top*: white noise added to the image as in **a**. *Bottom*: occlusion of the image as in **b**. We see the linear reconstruction fails, while Algorithm 2 recovers well, albeit with some blurring that can be interpreted as a consequence of entropic regularization.

Experimental Setup:

1. **Select μ_0** : Select a digit μ_0 **a.** generate a white noise image ζ . Set $\tilde{\mu}_0$ to be $\tilde{\mu}_0 = (1 - \alpha)\mu_0 + \alpha\zeta$. **b.** Set $\tilde{\mu}_0$ to be μ_0 with the central 8×8 square removed, and renormalized.
2. **Select $\{\mu_i\}_{i=1}^p$** : Select a set of images of the same digit as μ_0 to serve as the reference measures. **a.** Let $\tilde{\mu}_i = (1 - \alpha)\mu_0 + \alpha\mathbb{E}[\zeta]$. **b.** Let $\tilde{\mu}_i$ be μ_i with the central 8×8 square removed, and renormalized
3. **Estimate A, λ** : Use Algorithm 2 to compute the approximate Gram matrix \hat{A} using $\tilde{\mu}_0, \tilde{\mu}_1, \dots, \tilde{\mu}_p$ and then compute estimated coordinates $\hat{\lambda}$.
4. **Compute $\hat{\nu}_\lambda$** : Output $\hat{\mu}_0 = \nu_{\hat{\lambda}}$, where the barycenter is reconstructed from μ_1, \dots, μ_p .

An illustration of the procedure is shown in Figure 4. To recover the barycenter we use the method of [7]. As a competitive baseline we compare to a well-known existing method for histogram regression [9] in this setting. Our results are summarized in Table 1. We note that our method is over an order of magnitude faster than [9] on this dataset and achieves competitive results. This is particularly remarkable because [9] is specifically adapted to measures with structured support such as grids and meshes, while our Algorithm 2 is much more general.

4.4 Document Classification

Finally we consider the task of identifying the topic of a document using its word embedding representation as the empirical distribution. We assume that there are t topics and that we have p reference documents about each topic. Each document can be represented as a high-dimensional empirical measure using a combination of a bag-of-words representation

	[9], $\epsilon = 10$	Alg. 2, $\epsilon = 10$	Alg. 2, $\epsilon = 0$
Occlusion	2.5101 (2228s)	2.5488 (3.371s)	2.5287 (1.062s)
Noise ($\alpha = 0.5$)	2.4058 (2391s)	2.6797 (86.32s)	2.3787 (50.67s)

Table 1: Average quality of recovery of μ_0 measured in $W_2^2(\mu_0, \hat{\mu}_0)$ when reconstructing 500 random 4’s using a barycenter constructed from 10 random 4’s, as well as run times of each method. Algorithm 2 affords comparably accurate reconstructions in orders-of-magnitude faster time than the state-of-the-art [9].

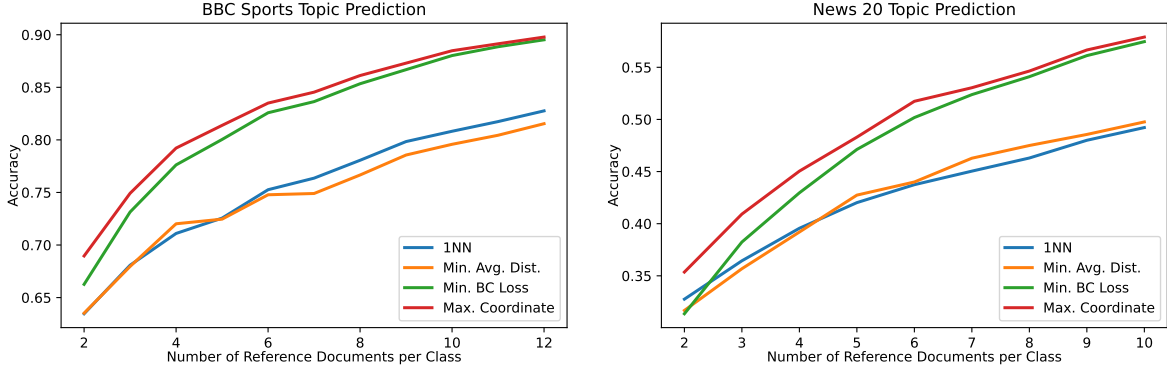


Figure 5: Document topic prediction accuracy as a function of number of reference documents in each class. *Top*: BBC Sport dataset (5 classes). *Bottom*: News20 dataset (20 classes).

and a node2vec [31] word-embedding, and is paired with topic label. We use the publicly available dataset provided by [24]. The task is to use a small number of labelled documents from each topic to predict the topic of a test document.

We consider four predictors: (1) **1-Nearest Neighbor (1NN)** which classifies using the topic of the W_2^2 -nearest reference document; (2) **Minimum Average Distance** which selects the topic with reference documents on average W_2^2 -closest to the test document; (3) **Minimum Barycenter Loss** which runs Algorithm 2 using the references from each topic separately and selects the topic with the smallest loss in the quadratic form; (4) **Maximum Coordinate** which runs Algorithm 2 using all the reference documents and chooses the topic which receives the most mass from $\hat{\lambda}$.

Our findings on the BBCSport (5 topics) and News20 (20 topics) datasets are reported in Figure 5. To generate these figures we randomly sample k reference documents per topic and a test set of 100 random documents. We apply the four methods listed above and compute the accuracy on the test set. This procedure is repeated 50 times for each choice of k and the average accuracy is plotted. See Supplementary Material Section 5.2 for details.

We see that even with a very small amount of training data, our BCM approaches perform well. Importantly, the BCM is able to represent unseen documents using these small training sets, giving it a clear advantage over simply classifying based on which document class it is W_2^2 -nearest (1NN) or W_2^2 -nearest in an aggregate sense (Min. Avg. Dist.). This suggests that even when p is small, the BCM has high modeling capacity and that the learned barycentric coordinates encode important information.

5 Conclusion

We have proposed a new method for computing coordinates under the BCM, together with guarantees on its solution via a convex program (Theorem 1) with closed-form coordinates in the Gaussian case (Corollary 1). We further developed an algorithm for estimating the coordinates under the BCM when all measures are accessible only via i.i.d. samples (Algorithm 1) which enjoys a natural smoothness and dimension-dependent rate of convergence to the true parameters (Theorem 2, Corollary 2). The BCM paradigm affords significant gains in runtime and robustness for barycenter parameterized Gaussian measure estimation, and provides an effective approach to image reconstruction and document classification when interpreting these data as measures. The results in this paper suggest the efficiency and effectiveness of the BCM as a broadly viable modelling tool.

Future Work and Open Questions: Section 3 provides a consistency analysis for A and λ by estimating the transport maps between each measure. But, all that is needed is an *estimate on the inner product* between the displacement maps, which in principle could admit more sample efficient approaches that avoid explicitly estimating the maps.

Section 4 suggests that unseen data can be well-represented in the BCM for randomly chosen reference measures. An interesting theoretical problem is to understand the representational capacity of the BCM using particular reference measures (e.g., random ones, optimally chosen ones, those in certain parametric families). This naturally touches on the question of the smoothness of the synthesis map $\lambda \mapsto \nu_\lambda$.

Computationally, all of our real data experiments use randomly chosen reference measures. It is of interest to develop efficient procedures as in [42] for *learning* reference measures that induce low reconstruction error. Beyond that, one could regularize the analysis problem (3) to encourage sparse or otherwise structured coordinates as is well-studied in Euclidean settings [2].

Acknowledgements

MW was partially supported by NSF CCF 1553075 and NSF CCF 1934553. RJ was partially supported by NSF DRL 1931978. SA was partially supported by NSF CCF 1553075, NSF DRL 1931978, NSF EEC 1937057, and AFOSR FA9550-18-1-0465. JMM was partially supported by NSF DMS 1912737, NSF DMS 1924513, and The Camille & Henry Dreyfus Foundation.

References

- [1] Martial Agueh and Guillaume Carlier. Barycenters in the Wasserstein space. *SIAM Journal on Mathematical Analysis*, 43(2):904–924, 2011.
- [2] Michal Aharon, Michael Elad, and Alfred Bruckstein. K-svd: An algorithm for designing overcomplete dictionaries for sparse representation. *IEEE Transactions on Signal Processing*, 54(11):4311–4322, 2006.

- [3] Jason M. Altschuler, Sinho Chewi, Patrik Gerber, and Austin J. Stromme. Averaging on the Bures-Wasserstein manifold: dimension-free convergence of gradient descent. In *Advances in Neural Information Processing Systems*, volume 34, 2021.
- [4] Pedro C. Álvarez-Esteban, E. Del Barrio, JA Cuesta-Albertos, and C Matrán. A fixed-point approach to barycenters in Wasserstein space. *Journal of Mathematical Analysis and Applications*, 441(2):744–762, 2016.
- [5] Luigi Ambrosio, Nicola Gigli, and Giuseppe Savare. *Gradient Flows: In Metric Spaces and in the Space of Probability Measures*. Lectures in Mathematics. ETH Zürich. Birkhäuser Basel, 2005.
- [6] Michael Bartholomew-Biggs, Steven Brown, Bruce Christianson, and Laurence Dixon. Automatic differentiation of algorithms. *Journal of Computational and Applied Mathematics*, 124:171–190, 12 2000.
- [7] Jean-David Benamou, Guillaume Carlier, Marco Cuturi, Luca Nenna, and Gabriel Peyré. Iterative Bregman projections for regularized transportation problems. *SIAM Journal on Scientific Computing*, 37(2):A1111–A1138, 2015.
- [8] Jérémie Bigot and Thierry Klein. Characterization of barycenters in the Wasserstein space by averaging optimal transport maps. *ESAIM: Probability and Statistics*, 22:35–57, 2018.
- [9] Nicolas Bonneel, Gabriel Peyré, and Marco Cuturi. Wasserstein Barycentric Coordinates: Histogram Regression Using Optimal Transport. *ACM Transactions on Graphics*, 35(4):71:1–71:10, 2016.
- [10] Nicolas Bonneel, Julien Rabin, Gabriel Peyré, and Hanspeter Pfister. Sliced and Radon Wasserstein barycenters of measures. *Journal of Mathematical Imaging and Vision*, 51(1):22–45, 2015.
- [11] Yann Brenier. Polar factorization and monotone rearrangement of vector-valued functions. *Communications on Pure and Applied Mathematics*, 44(4):375–417, 1991.
- [12] Kevin Cheng, Shuchin Aeron, Michael C Hughes, and Eric Miller. Dynamical Wasserstein barycenters for time-series modeling. In *Advances in Neural Information Processing Systems*, volume 34, 2021.
- [13] Sinho Chewi, Tyler Maunu, Philippe Rigollet, and Austin J Stromme. Gradient descent algorithms for Bures-Wasserstein barycenters. In *Conference on Learning Theory*, pages 1276–1304. PMLR, 2020.
- [14] Lenaïc Chizat, Pierre Roussillon, Flavien Léger, François-Xavier Vialard, and Gabriel Peyré. Faster Wasserstein distance estimation with the Sinkhorn divergence. *arXiv preprint arXiv:2006.08172*, 2020.
- [15] Sebastian Clatici, Edward Chien, and Justin Solomon. Stochastic wasserstein barycenters. In *International Conference on Machine Learning*, pages 999–1008. PMLR, 2018.

- [16] Pierre Colombo, Guillaume Staerman, Chloe Clavel, and Pablo Piantanida. Automatic text evaluation through the lens of Wasserstein barycenters. *arXiv preprint arXiv:2108.12463*, 2021.
- [17] Marco Cuturi. Sinkhorn distances: Lightspeed computation of optimal transport. *Advances in neural information processing systems*, 26:2292–2300, 2013.
- [18] Marco Cuturi and Arnaud Doucet. Fast computation of wasserstein barycenters. In *International conference on machine learning*, pages 685–693. PMLR, 2014.
- [19] Nabarun Deb, Promit Ghosal, and Bodhisattva Sen. Rates of estimation of optimal transport maps using plug-in estimators via barycentric projections. *Advances in Neural Information Processing Systems*, 34, 2021.
- [20] David L Donoho. Compressed sensing. *IEEE Transactions on information theory*, 52(4):1289–1306, 2006.
- [21] Maurice Fréchet. Les éléments aléatoires de nature quelconque dans un espace distancié. *Annales de l’institut Henri Poincaré*, 10(4):215–310, 1948.
- [22] Aude Genevay. *Entropy-regularized optimal transport for machine learning*. PhD thesis, Paris Sciences et Lettres (ComUE), 2019.
- [23] Florian F. Gunsilius. On the convergence rate of potentials of brenier maps. *Econometric Theory*, page 1–37, 2021.
- [24] Gao Huang, Chuan Quo, Matt J Kusner, Yu Sun, Kilian Q Weinberger, and Fei Sha. Supervised word mover’s distance. In *Proceedings of the 30th International Conference on Neural Information Processing Systems*, pages 4869–4877, 2016.
- [25] Jan-Christian Hütter and Philippe Rigollet. Minimax estimation of smooth optimal transport maps. *The Annals of Statistics*, 49(2):1166–1194, 2021.
- [26] Hermann Karcher. Riemannian center of mass and mollifier smoothing. *Communications on Pure and Applied Mathematics*, 30(5):509–541, 1977.
- [27] Alexey Kroshnin, Nazarii Tupitsa, Darina Dvinskikh, Pavel Dvurechensky, Alexander Gasnikov, and Cesar Uribe. On the complexity of approximating Wasserstein barycenters. In *International conference on machine learning*, pages 3530–3540. PMLR, 2019.
- [28] Yann LeCun. The MNIST database of handwritten digits. <http://yann.lecun.com/exdb/mnist/>, 1998.
- [29] Stéphane Mallat. *A wavelet tour of signal processing*. Elsevier, 1999.
- [30] Robert J McCann. A convexity principle for interacting gases. *Advances in Mathematics*, 128(1):153–179, 1997.
- [31] Tomas Mikolov, Ilya Sutskever, Kai Chen, Greg S Corrado, and Jeff Dean. Distributed representations of words and phrases and their compositionality. In *Advances in neural information processing systems*, pages 3111–3119, 2013.

- [32] Eduardo Fernandes Montesuma and Fred Maurice Ngole Mboula. Wasserstein barycenter for multi-source domain adaptation. In *IEEE/CVF Conference on Computer Vision and Pattern Recognition*, pages 16785–16793, 2021.
- [33] Kevin P Murphy. *Machine learning: a probabilistic perspective*. MIT press, 2012.
- [34] Antoni Musolas, Steven T Smith, and Youssef Marzouk. Geodesically parameterized covariance estimation. *SIAM Journal on Matrix Analysis and Applications*, 42(2):528–556, 2021.
- [35] Victor M Panaretos and Yoav Zemel. *An invitation to statistics in Wasserstein space*. Springer Nature, 2020.
- [36] Gabriel Peyré and Marco Cuturi. Computational optimal transport, 2020.
- [37] Aram-Alexandre Pooladian and Jonathan Niles-Weed. Entropic estimation of optimal transport maps. *arXiv: 2109.12004*, 2021.
- [38] Tiberiu Popoviciu. Sur les équations algébriques ayant toutes leurs racines réelles. *Mathematica*, 9:129–145, 1935.
- [39] Julien Rabin, Gabriel Peyré, Julie Delon, and Marc Bernot. Wasserstein barycenter and its application to texture mixing. In *International Conference on Scale Space and Variational Methods in Computer Vision*, pages 435–446. Springer, 2011.
- [40] Ievgen Redko, Nicolas Courty, Rémi Flamary, and Devis Tuia. Optimal transport for multi-source domain adaptation under target shift. In *The 22nd International Conference on Artificial Intelligence and Statistics*, pages 849–858. PMLR, 2019.
- [41] F. Santambrogio. *Optimal Transport for Applied Mathematicians: Calculus of Variations, PDEs, and Modeling*. Progress in Nonlinear Differential Equations and Their Applications. Springer International Publishing, 2015.
- [42] Morgan A Schmitz, Matthieu Heitz, Nicolas Bonneel, Fred Ngole, David Coeurjolly, Marco Cuturi, Gabriel Peyré, and Jean-Luc Starck. Wasserstein dictionary learning: Optimal transport-based unsupervised nonlinear dictionary learning. *SIAM Journal on Imaging Sciences*, 11(1):643–678, 2018.
- [43] Hans Schwerdtfeger. *Introduction to linear algebra and the theory of matrices*. P. Noordhoff, 1961.
- [44] Sidak Pal Singh, Andreas Hug, Aymeric Dieuleveut, and Martin Jaggi. Context mover’s distance & barycenters: Optimal transport of contexts for building representations. In *International Conference on Artificial Intelligence and Statistics*, pages 3437–3449. PMLR, 2020.
- [45] Ivana Tošić and Pascal Frossard. Dictionary learning. *IEEE Signal Processing Magazine*, 28(2):27–38, 2011.
- [46] Cedric Villani. *Topics in Optimal Transportation*. Graduate studies in mathematics. American Mathematical Society, 2003.

- [47] Hongteng Xu, Wenlin Wang, Wei Liu, and Lawrence Carin. Distilled Wasserstein learning for word embedding and topic modeling. In *Advances in Neural Information Processing Systems*, pages 1716–1725, 2018.
- [48] Lei Yang, Jia Li, Defeng Sun, and Kim-Chuan Toh. A fast globally linearly convergent algorithm for the computation of Wasserstein barycenters. *Journal of Machine Learning Research*, 22(21):1–37, 2021.

Supplementary Material

1 Precise Statements of Technical Results

For completeness, we replicate the theorem describing conditions under which Karcher means are guaranteed to be barycenters.

Theorem 3. ([35], Theorem 3.1.15) *Let $\lambda \in \Delta^p$ with $\lambda_i \neq 0$ for all i . Let $\Omega \subset \mathbb{R}^d$ be open and convex and let $\mu_1, \dots, \mu_p \in \mathcal{P}_{2,\text{ac}}(\mathbb{R}^d)$ supported on Ω with bounded, strictly positive densities g_1, \dots, g_p . Suppose that μ_0 is an absolutely continuous Karcher mean for λ and is supported on Ω with bounded strictly positive density f there. Then μ_0 is the Wasserstein barycenter for coordinates λ if one of the following holds:*

- (1) $\Omega = \mathbb{R}^d$ and the densities f, g_1, \dots, g_p are locally Hölder continuous.
- (2) Ω is bounded and the densities f, g_1, \dots, g_p are bounded below on Ω .

Next we include a technical theorem which we will leverage in our proof of the convergence of the entries A_{ij} . Before doing so, we introduce the necessary background.

Theorem 4. ([11]) *Let $\mu \in \mathcal{P}_{2,\text{ac}}(\mathbb{R}^d)(\Omega)$ and $\nu \in \mathcal{P}(\Omega)$. Then*

- 1. *There exists a solution T_0 to (1), with $T_0 = \nabla \varphi_0$, for a convex function φ_0 solving*

$$\inf_{\varphi \in L^1(\mu)} \int \varphi d\mu + \int \varphi^* d\nu$$

where φ^ is the convex conjugate of φ_0 .*

- 2. *If in addition $Q \in \mathcal{P}_{2,\text{ac}}(\mathbb{R}^d)(\Omega)$, then $\nabla \varphi_0^*$ is an admissible optimal transport map from Q to P .*

Let \mathcal{C}^α denote the space of functions possessing $\lfloor \alpha \rfloor$ continuous derivatives and whose $\lfloor \alpha \rfloor$ 'th derivative is $(\alpha - \lfloor \alpha \rfloor)$ Hölder smooth. Using these conventions, we require the technical conditions:

A4. $\mu, \nu \in \mathcal{P}_{2,\text{ac}}(\Omega)$ for a compact set Ω , with densities satisfying $p(x), q(x) \leq M$ and $q(x) \geq m > 0$ for all $x \in \Omega$.

A5. $\varphi_0 \in \mathcal{C}^2(\Omega)$ and $\varphi_0^* \in \mathcal{C}^{\alpha+1}(\Omega)$ for $\alpha > 1$.

A6. There exist $l, L > 0$ such that $T_0 = \nabla \varphi_0$, with $lI \preceq \nabla^2 \varphi_0(x) \preceq LI$ for all $x \in \Omega$.

This first assumption is a specialization of **A1** and **A2**, restricting to the case where Ω is compact. The latter two can be thought of as regularity conditions on the optimal transport maps between base and reference measures. **A5** asserts that the optimal maps have smooth derivatives and **A6** controls the derivatives from both above and below.

1.1 Properties of The Entropic Map

Let $X_i \sim \mu_0, Y_i \sim \mu_1$ for $i = 1, \dots, n$ be i.i.d. samples from their respective distributions. From these samples construct the empirical measures $\hat{\mu}_{0,n} = \frac{1}{n} \sum_{i=1}^n \delta_{X_i}$ and $\hat{\mu}_{1,n} = \frac{1}{n} \sum_{i=1}^n \delta_{Y_i}$.

For $\epsilon > 0$ and n samples from each measures, the discrete entropically regularized OT problem can be written

$$\min_{\substack{\pi \in \mathbb{R}_+^{n \times n} \\ \pi \mathbf{1} = (1/n) \mathbf{1} \\ \pi^T \mathbf{1} = (1/n) \mathbf{1}}} \sum_{j,k=1}^n \pi_{jk} \|X_j - Y_k\|_2^2 + \epsilon \pi_{jk} \log \pi_{jk}$$

This problem has a dual formulation [22] given by

$$\max_{f,g \in \mathbb{R}^n} \frac{1}{n} \sum_{i=1}^n f_i + g_i - \epsilon \langle e^{f/\epsilon}, K e^{g/\epsilon} \rangle$$

where $K_{i,j} = \exp(-\|X_i - Y_j\|_2^2/\epsilon)$. g_ϵ is defined to be the optimal g in the maximization above, parameterized by the setting of $\epsilon > 0$.

One of the primary motivations for selecting the entropic map as our map estimate is that g_ϵ can be efficiently computed [36], and it comes with the performance guarantee stated below.

In the following theorem the constants may depend on the dimension d , the diameter of the support $|\Omega|$, M, m, l, L , and $\|\varphi_0^*\|_{C^{\alpha+1}}$.

Theorem 5. ([37] Theorem 3) Under **A4, A5, A6**, the entropic map $\hat{T} = T_{\epsilon, (n, n)}$ from $\hat{\mu}_n$ to $\hat{\nu}_n$ with regularization parameter $\epsilon \asymp n^{-1/(d' + \bar{\alpha} + 1)}$ satisfies

$$\mathbb{E} \|\hat{T} - T_0\|_{L^2(\mu)}^2 \lesssim (1 + I_0(\mu, \nu)) n^{-\frac{(\bar{\alpha} + 1)}{2(d' + \bar{\alpha} + 1)}} \log n \quad (9)$$

where $d' = 2\lceil d/2 \rceil$ and $\bar{\alpha} = \min(\alpha, 3)$ and $I_0(\mu, \nu)$ is the integrated Fisher information between μ and ν .

For more information on $I_0(\mu, \nu)$ see [14]. We remark that when $\alpha \geq 2$ then under **A4, A5, A6**, it has been shown $I_0(\mu, \nu) \leq C$ for a positive constant C [14]. The notation $a \asymp b$ means that there exists positive constants c, C such that $ca \leq b \leq Ca$ and $a \lesssim b$ means that there is a positive constant C such that $a \leq Cb$.

2 Proofs of Theoretical Results

2.1 Proof of Proposition 1

Proof. We first apply the definitions given in Section 2 and leverage (4):

$$\begin{aligned} \|\nabla G_\lambda(\mu_0)\|_{\mu_0}^2 &= \left\| - \sum_{i=1}^p \lambda_i (T_{\mu_0 \rightarrow \mu_i} - \text{Id}) \right\|_{\mu_0}^2 \\ &= \int_{\mathbb{R}^d} \left\langle \sum_{i=1}^p \lambda_i (T_{\mu_0 \rightarrow \mu_i} - \text{Id}), \sum_{j=1}^p \lambda_j (T_{\mu_0 \rightarrow \mu_j} - \text{Id}) \right\rangle d\mu_0 \\ &= \int_{\mathbb{R}^d} \sum_{i,j=1}^p \lambda_i \lambda_j \langle T_{\mu_0 \rightarrow \mu_i} - \text{Id}, T_{\mu_0 \rightarrow \mu_j} - \text{Id} \rangle d\mu_0 \end{aligned}$$

$$= \sum_{i,j=1}^p \lambda_i \lambda_j A_{ij} = \lambda^T A \lambda.$$

To establish the convexity of the function in terms of λ , it is sufficient to show that A is symmetric positive semi-definite. Observe that A is a Gram matrix of the set $\{T_{\mu_0 \rightarrow \mu_i} - \text{Id}\}_{i=1}^p \subset T_{\mu_0} \mathcal{P}_{2,\text{ac}}(\mathbb{R}^d)$ with the inner product in $T_{\mu_0} \mathcal{P}_{2,\text{ac}}(\mathbb{R}^d)$. It is classical that all Gram matrices are symmetric positive semi-definite [43] and this completes the proof. \square

2.2 Proof of Theorem 1

Proof. The convexity of the objective is established in Proposition 1, and the feasible set Δ^p is trivially convex.

By Theorem 3, when assumptions **A1-A3**, all Karcher means are barycenters, and therefore $\mu_0 = \nu_\lambda$, and it is always the case that barycenters are Karcher means. Therefore it is sufficient to check that the minimum value is 0 if and only if μ_0 is a Karcher mean.

In the case that the minimum is zero, there is some λ_* such that $(\lambda_*)^T A \lambda_* = 0$ and we can apply Proposition 1 to show that μ_0 is a Karcher mean for λ_* . Similarly if μ_0 is a Karcher mean for some λ_* by definition we have $\|\nabla G_{\lambda_*}(\mu_0)\|_{\mu_0}^2 = 0$ and again by Proposition 1 we have that λ_* achieves the minimum of zero in the optimization. \square

2.3 Proof of Corollary 1

Proof. **A1,A2,A3** are clearly satisfied in the Gaussian case with $\Omega = \mathbb{R}^d$ since the pdf of a non-degenerate multivariate Gaussian is positive everywhere and Lipschitz continuous. Furthermore the barycenter of zero-mean Gaussians is itself a zero-mean Gaussian [1] Theorem 6.1.

Therefore we can apply Theorem 1 and all that remains is to calculate A_{ij} as follows. Noting that the C_i are all symmetric [1] we have

$$\begin{aligned} A_{ij} &= \int_{\mathbb{R}^d} \langle (T_i(x) - \text{Id}(x)), (T_j(x) - \text{Id}(x)) \rangle dS_0(x) \\ &= \int_{\mathbb{R}^d} \langle (C_i - I)x, (C_j - I)x \rangle dS_0(x) & (\text{Eq. 6}) \\ &= \mathbb{E}_{X \sim \mathcal{N}(0, S_0)} \left[X^T (C_i - I)^T (C_j - I) X \right] \\ &= \mathbb{E}_{X \sim \mathcal{N}(0, S_0)} \left[X^T (C_i - I) (C_j - I) X \right] & (C_i \text{ all sym.}) \\ &= \text{Tr}((C_i - I)(C_j - I)S_0). \end{aligned}$$

The last equality comes from the identity $\mathbb{E}_{X \sim \mathcal{N}(0, S)} [X^T B X] = \text{Tr}(BS)$ which holds for all $B \in \mathbb{R}^{d \times d}$ and $S \in \mathbb{S}_{++}^d$. \square

2.4 Exact Statement and Proof of Theorem 2

Theorem 6. (Convergence Rate of A_{ij}) Let T_1, T_2 be the optimal transport maps from μ_0 to μ_1, μ_2 respectively. Suppose that **A4**, **A5**, **A6** are satisfied for both pairs (μ_0, μ_1) and (μ_0, μ_2) . Let $X_1, \dots, X_{2n} \sim \mu_0, Y_1, \dots, Y_n \sim \mu_1, Z_1, \dots, Z_n \sim \mu_2$. Let \hat{T}_1 and \hat{T}_2 be the entropic maps from μ_0 to μ_1 and μ_2 respectively, both with $\epsilon \asymp n^{-1/(d'+\bar{\alpha}+1)}$ and computed using X_1, \dots, X_n . Then we have

$$\mathbb{E} \left[\left| \int \langle T_1 - Id, T_2 - Id \rangle d\mu_0 - \frac{1}{n} \sum_{i=n+1}^{2n} \langle \hat{T}_1(X_i) - X_i, \hat{T}_2(X_i) - X_i \rangle \right| \right] \quad (10)$$

$$\lesssim \frac{1}{\sqrt{n}} + n^{-\frac{\bar{\alpha}+1}{4(d'+\bar{\alpha}+1)}} \sqrt{\log n} \sqrt{1 + I_0(\mu_0, \mu_1) + I_0(\mu_0, \mu_2)} \quad (11)$$

where $d' = \lceil d/2 \rceil$, $\bar{\alpha} = \alpha \wedge 3$ and $I_0(\mu_0, \mu_1)$ is the integrated Fisher information along the Wasserstein geodesic between μ and μ_1 .

Before we begin the proof, we remark that by writing μ_i, μ_j instead of μ_1, μ_2 , the random variable in the expectation is just $|A_{ij} - \hat{A}_{ij}|$ and therefore this result allows us to control the entry-wise deviations of \hat{A}_{ij} from their true values.

Proof. Throughout, unless otherwise noted, the expectation is with respect to all of $X_1, \dots, X_{2n}, Y_1, \dots, Y_n$ and Z_1, \dots, Z_n . We also use the notations X^n to denote the set of variables (X_1, \dots, X_n) , and similarly for Y^n and Z^n .

First observe that we can assume without loss of generality that $0 \in \Omega$; see [36] Remark 2.9 for invariance of T_1, T_2 under translation. For the translation invariance of \hat{T}_1, \hat{T}_2 , observe that both obtaining g_ϵ , and evaluating \hat{T}_1, \hat{T}_2 at fixed points, requires only the distances $\|X_i - Y_j\|_2^2 = \|(X_i - t) - (Y_j - t)\|_2^2$.

$$\begin{aligned} & \mathbb{E} \left[\left| \int \langle T_1 - Id, T_2 - Id \rangle d\mu_0 - \frac{1}{n} \sum_{i=n+1}^{2n} \langle \hat{T}_1(X_i) - X_i, \hat{T}_2(X_i) - X_i \rangle \right| \right] \\ &= \mathbb{E} \left[\left| \int \langle T_1 - Id, T_2 - Id \rangle d\mu_0 - \frac{1}{n} \sum_{i=n+1}^{2n} \langle T_1(X_i) - X_i, T_2(X_i) - X_i \rangle \right. \right. \\ & \quad \left. \left. + \frac{1}{n} \sum_{i=n+1}^{2n} \langle T_1(X_i) - X_i, T_2(X_i) - X_i \rangle - \frac{1}{n} \sum_{i=n+1}^{2n} \langle \hat{T}_1(X_i) - X_i, \hat{T}_2(X_i) - X_i \rangle \right| \right] \\ &\leq \mathbb{E} \left[\left| \int \langle T_1 - Id, T_2 - Id \rangle d\mu_0 - \frac{1}{n} \sum_{i=n+1}^{2n} \langle T_1(X_i) - X_i, T_2(X_i) - X_i \rangle \right| \right] \\ & \quad + \mathbb{E} \left[\left| \frac{1}{n} \sum_{i=n+1}^{2n} \langle T_1(X_i) - X_i, T_2(X_i) - X_i \rangle - \frac{1}{n} \sum_{i=n+1}^{2n} \langle \hat{T}_1(X_i) - X_i, \hat{T}_2(X_i) - X_i \rangle \right| \right] \end{aligned}$$

We consider the first and second terms separately. For brevity, let h be the function defined by

$$h(x) = \langle T_1(x) - x, T_2(x) - x \rangle.$$

Note that h is bounded on Ω since

$$|h(x)| = |\langle T_1(x) - x, T_2(x) - x \rangle| \leq \|T_1(x) - x\|_2 \|T_2(x) - x\|_2 \leq (2|\Omega|)(2|\Omega|) = 4|\Omega|^2,$$

which implies by Popoviciu's inequality [38] that $\text{Var}[h(X)] \leq 16|\Omega|^4$. From this it follows

$$\begin{aligned} & \mathbb{E} \left[\left| \int \langle T_1 - Id, T_2 - Id \rangle d\mu_0 - \frac{1}{n} \sum_{i=n+1}^{2n} \langle T_1(X_i) - X_i, T_2(X_i) - X_i \rangle \right| \right] \\ &= \mathbb{E} \left[\left| \mathbb{E}_{X \sim \mu_0}[h(X)] - \frac{1}{n} \sum_{i=n+1}^{2n} h(X_i) \right| \right] \\ &\leq \sqrt{\frac{\text{Var}[h(X)]}{n}} \leq \sqrt{\frac{16|\Omega|^4}{n}} \lesssim \frac{1}{\sqrt{n}} \end{aligned}$$

where we have used that for all i.i.d. random variables U, U_1, \dots, U_n with finite variance

$$\mathbb{E}[|\mathbb{E}[U] - \frac{1}{n} \sum_{i=1}^n U_i|] \leq \sqrt{\frac{\text{Var}[U]}{n}}.$$

We now handle the second term:

$$\begin{aligned} & \mathbb{E} \left[\left| \frac{1}{n} \sum_{i=n+1}^{2n} \langle T_1(X_i) - X_i, T_2(X_i) - X_i \rangle - \frac{1}{n} \sum_{i=n+1}^{2n} \langle \hat{T}_1(X_i) - X_i, \hat{T}_2(X_i) - X_i \rangle \right| \right] \\ &\leq \frac{1}{n} \sum_{i=n+1}^{2n} \mathbb{E} \left[\left| \langle T_1(X_i) - X_i, T_2(X_i) - X_i \rangle - \langle \hat{T}_1(X_i) - X_i, \hat{T}_2(X_i) - X_i \rangle \right| \right] \\ &= \mathbb{E} \left[\left| \langle T_1(X_{n+1}) - X_{n+1}, T_2(X_{n+1}) - X_{n+1} \rangle - \langle \hat{T}_1(X_{n+1}) - X_{n+1}, \hat{T}_2(X_{n+1}) - X_{n+1} \rangle \right| \right] \\ &= \mathbb{E} \left[\left| \langle T_1(X_{n+1}), T_2(X_{n+1}) \rangle - \langle \hat{T}_1(X_{n+1}), \hat{T}_2(X_{n+1}) \rangle \right. \right. \\ &\quad \left. \left. + \langle \hat{T}_1(X_{n+1}) - T_1(X_{n+1}), X_{n+1} \rangle + \langle \hat{T}_2(X_{n+1}) - T_2(X_{n+1}), X_{n+1} \rangle \right| \right] \\ &\leq \mathbb{E} \left[\left| \langle T_1(X_{n+1}), T_2(X_{n+1}) \rangle - \langle \hat{T}_1(X_{n+1}), \hat{T}_2(X_{n+1}) \rangle \right| \right] \\ &\quad + \mathbb{E} \left[\left| \langle \hat{T}_1(X_{n+1}) - T_1(X_{n+1}), X_{n+1} \rangle \right| \right] + \mathbb{E} \left[\left| \langle \hat{T}_2(X_{n+1}) - T_2(X_{n+1}), X_{n+1} \rangle \right| \right] \end{aligned}$$

Here we can control the three terms separately. We first take care of the middle term and the last term follows by an identical argument.

$$\begin{aligned} & \mathbb{E} \left[\left| \langle \hat{T}_1(X_{n+1}) - T_1(X_{n+1}), X_{n+1} \rangle \right| \right] \\ &= \mathbb{E}_{X^n, Y^n, X_{n+1}} \left[\left| \langle \hat{T}_1(X_{n+1}) - T_1(X_{n+1}), X_{n+1} \rangle \right| \right] \\ &\leq \mathbb{E}_{X^n, Y^n, X_{n+1}} \left[\| \hat{T}_1(X_{n+1}) - T_1(X_{n+1}) \|_2 \| X_{n+1} \|_2 \right] \quad (\text{Cauchy-Schwarz}) \\ &\leq |\Omega| \mathbb{E}_{X^n, Y^n, X_{n+1}} \left[\| \hat{T}_1(X_{n+1}) - T_1(X_{n+1}) \|_2 \right] \quad (\| X_{n+1} \| \leq |\Omega|) \\ &= |\Omega| \mathbb{E}_{X^n, Y^n, X_{n+1}} \left[\mathbb{E}_{X_{n+1}} \| \hat{T}_1(X_{n+1}) - T_1(X_{n+1}) \|_2 \right] \\ &= |\Omega| \mathbb{E}_{X^n, Y^n, X_{n+1}} \left[\mathbb{E}_{X_{n+1}} \sqrt{\| \hat{T}_1(X_{n+1}) - T_1(X_{n+1}) \|_2^2} \right] \end{aligned}$$

$$\begin{aligned}
&\leq |\Omega| \mathbb{E}_{X^n, Y^n, X_{n+1}} \left[\sqrt{\mathbb{E}_{X_{n+1}} \|\hat{T}_1(X_{n+1}) - T_1(X_{n+1})\|_2^2} \right] & (\text{Jensen}) \\
&= |\Omega| \mathbb{E}_{X^n, Y^n} \left[\|\hat{T}_1 - T_1\|_{L^2(\mu_0)} \right] \\
&\leq |\Omega| \sqrt{\mathbb{E}_{X^n, Y^n} \left[\|\hat{T}_1 - T_1\|_{L^2(\mu_0)}^2 \right]} \\
&\lesssim \sqrt{(1 + I_0(\mu_0, \mu_1)) n^{-\frac{\bar{\alpha}+1}{2(d'+\bar{\alpha}+1)}} \log(n)}. & (\text{Theorem Above})
\end{aligned}$$

As mentioned above the third term is exactly the same except replacing T_1 and \hat{T}_1 with T_2 and \hat{T}_2 as well as Y^n with Z^n .

To control the first term we start with a different trick and then end up following the same pattern as in the bound above.

$$\begin{aligned}
&\mathbb{E} \left[\left| \langle T_1(X_{n+1}), T_2(X_{n+1}) \rangle - \langle \hat{T}_1(X_{n+1}), \hat{T}_2(X_{n+1}) \rangle \right| \right] \\
&= \mathbb{E} \left[\left| \langle T_1(X_{n+1}) - \hat{T}_1(X_{n+1}), T_2(X_{n+1}) \rangle - \langle \hat{T}_1(X_{n+1}), T_2(X_{n+1}) - \hat{T}_2(X_{n+1}) \rangle \right| \right] \\
&\leq \mathbb{E} \left[\left| \langle T_1(X_{n+1}) - \hat{T}_1(X_{n+1}), T_2(X_{n+1}) \rangle \right| \right] + \mathbb{E} \left[\left| \langle \hat{T}_1(X_{n+1}), T_2(X_{n+1}) - \hat{T}_2(X_{n+1}) \rangle \right| \right] \\
&\leq \mathbb{E} \left[\|T_1(X_{n+1}) - \hat{T}_1(X_{n+1})\|_2 \|T_2(X_{n+1})\| \right] + \mathbb{E} \left[\|\hat{T}_1(X_{n+1})\|_2 \|T_2(X_{n+1}) - \hat{T}_2(X_{n+1})\|_2 \right] \\
&\leq |\Omega| \mathbb{E} \left[\|T_1(X_{n+1}) - \hat{T}_1(X_{n+1})\|_2 \right] + |\Omega| \mathbb{E} \left[\|T_2(X_{n+1}) - \hat{T}_2(X_{n+1})\|_2 \right] \\
&= |\Omega| \mathbb{E}_{X^n, Y^n, X_{n+1}} \left[\|T_1(X_{n+1}) - \hat{T}_1(X_{n+1})\|_2 \right] + |\Omega| \mathbb{E}_{X^n, Z^n, X_{n+1}} \left[\|T_2(X_{n+1}) - \hat{T}_2(X_{n+1})\|_2 \right].
\end{aligned}$$

Above we have made use of the fact that both $T_2(X_1)$ and $\hat{T}_1(X_1)$ are contained in Ω which implies that $\|T_2(X_1)\|_2 \leq |\Omega|$. $T_2(X_1) \in \Omega$ follows from the fact that T_2 is a map from μ_0 to μ_2 . To see that $\|\hat{T}_1(X_1)\| \leq |\Omega|$, note that from equation (7) $\hat{T}_1(X_1)$ is a convex combination of $Y_1, \dots, Y_n \in \Omega$ and each of which satisfies $\|Y_i\|_2 \leq |\Omega|$.

Observe that both of the remaining terms above appear along the way of derivation above (the latter requiring again replacing T_1, \hat{T}_1 , and Y^n with T_2, \hat{T}_2 , and Z^n respectively).

Combining terms we have overall the following result

$$\begin{aligned}
&\mathbb{E} \left[\left| \int \langle T_1 - Id, T_2 - Id \rangle d\mu_0 - \frac{1}{n} \sum_{i=n+1}^{2n} \langle \hat{T}_1(X_i) - X_i, \hat{T}_2(X_i) - X_i \rangle \right| \right] \\
&\lesssim \frac{1}{\sqrt{n}} + 2\sqrt{(1 + I_0(\mu_0, \mu_1)) n^{-\frac{\bar{\alpha}+1}{2(d'+\bar{\alpha}+1)}} \log(n)} + 2\sqrt{(1 + I_0(\mu_0, \mu_2)) n^{-\frac{\bar{\alpha}+1}{2(d'+\bar{\alpha}+1)}} \log(n)} \\
&= \frac{1}{\sqrt{n}} + n^{-\frac{\bar{\alpha}+1}{4(d'+\bar{\alpha}+1)}} \sqrt{\log n} \left(\sqrt{1 + I_0(\mu_0, \mu_1)} + \sqrt{1 + I_0(\mu_0, \mu_2)} \right) \\
&\lesssim \frac{1}{\sqrt{n}} + n^{-\frac{\bar{\alpha}+1}{4(d'+\bar{\alpha}+1)}} \sqrt{\log n} \sqrt{1 + I_0(\mu_0, \mu_1) + I_0(\mu_0, \mu_2)}.
\end{aligned}$$

□

2.5 Proof of Corollary 2

Proof. Let B_n denote the entrywise bound in Theorem 2. Noting that $\hat{\lambda}^T \hat{A} \hat{\lambda} \leq \lambda_*^T \hat{A} \lambda_*$ by construction, we estimate

$$\begin{aligned}
\mathbb{E}[\hat{\lambda}^T A \hat{\lambda}] &= \mathbb{E}[\hat{\lambda}^T (A - \hat{A}) \hat{\lambda}] + \mathbb{E}[\hat{\lambda}^T \hat{A} \hat{\lambda}] \\
&\leq \mathbb{E}[|\hat{\lambda}^T (A - \hat{A}) \hat{\lambda}|] + \mathbb{E}[\lambda_*^T \hat{A} \lambda_*] \\
&= \mathbb{E}[|\hat{\lambda}^T (A - \hat{A}) \hat{\lambda}|] + \mathbb{E}[\lambda_*^T (\hat{A} - A) \lambda_*] \quad (\lambda_*^T A \lambda_* = 0) \\
&= \mathbb{E}\left[\left|\sum_{i,j=1}^p (\hat{\lambda})_i (\hat{\lambda})_j (A - \hat{A})_{ij}\right|\right] + \mathbb{E}\left[\left|\sum_{i,j=1}^p (\lambda_*)_i (\lambda_*)_j (A - \hat{A})_{ij}\right|\right] \\
&\leq \mathbb{E}\left[\sum_{i,j=1}^p (\hat{\lambda})_i (\hat{\lambda})_j |A_{ij} - \hat{A}_{ij}|\right] + \mathbb{E}\left[\sum_{i,j=1}^p (\lambda_*)_i (\lambda_*)_j |A_{ij} - \hat{A}_{ij}|\right] \\
&\leq 2 \mathbb{E}\left[\sum_{i,j=1}^p |A_{ij} - \hat{A}_{ij}|\right] \\
&= 2 \sum_{i,j=1}^p \mathbb{E}[|A_{ij} - \hat{A}_{ij}|] \\
&\lesssim 2p^2 B_n \quad (\text{Theorem 2})
\end{aligned}$$

Since A is positive semidefinite and by assumption $\lambda_* \in \Delta^p$ satisfies $\lambda_*^T A \lambda_* = 0$, it follows that λ_* is an eigenvector of A with eigenvalue 0. Let $0 < \alpha_2 \leq \dots \leq \alpha_p$ be the non-zero eigenvalues of A with associated orthonormal eigenvectors v_2, \dots, v_p . Orthogonally decompose $\hat{\lambda} = \hat{\beta} \lambda_* + \hat{\lambda}_\perp$, where $\hat{\beta} \in \mathbb{R}$ and $\hat{\lambda}_\perp$ is in the span of $\{v_2, \dots, v_p\}$. Note that $\hat{\beta}$ and $\hat{\lambda}_\perp$ are random. Then,

$$\begin{aligned}
\mathbb{E}[\|\hat{\lambda} - \hat{\beta} \lambda_*\|_2^2] &= \mathbb{E}[\|\hat{\lambda}_\perp\|_2^2] \\
&= \mathbb{E}\left[\sum_{i=2}^p |v_i^T \hat{\lambda}_\perp|^2\right] \\
&\leq \frac{1}{\alpha_2} \mathbb{E}\left[\sum_{i=2}^p \alpha_i |v_i^T \hat{\lambda}_\perp|^2\right] \\
&= \frac{1}{\alpha_2} \mathbb{E}[(\hat{\lambda}_\perp)^T A \hat{\lambda}_\perp] \\
&= \frac{1}{\alpha_2} \mathbb{E}[|\hat{\lambda}^T A \hat{\lambda}|] \\
&\lesssim \frac{2p^2}{\alpha_2} B_n.
\end{aligned}$$

Summing both sides of the equation $\hat{\lambda} = \hat{\beta} \lambda_* + \hat{\lambda}_\perp$ and recalling $\lambda_*, \hat{\lambda} \in \Delta^p$ yields

$$1 = \hat{\beta} + \sum_{j=1}^p (\hat{\lambda}_\perp)_j$$

$$\begin{aligned}
&\leq \hat{\beta} + \|\hat{\lambda}_\perp\|_1 \\
&\leq \hat{\beta} + \sqrt{p}\|\hat{\lambda}_\perp\|_2,
\end{aligned}$$

which implies that $\mathbb{E}[(1 - \hat{\beta})^2] \leq p\mathbb{E}[\|\hat{\lambda}_\perp\|_2^2] \lesssim \frac{2p^3}{\alpha_2}B_n$.

Finally, we use the fact that $\hat{\lambda} - \hat{\beta}\lambda_* = \hat{\lambda}_\perp$ and $(\hat{\beta} - 1)\lambda_*$ are orthogonal to bound:

$$\begin{aligned}
\mathbb{E}[\|\hat{\lambda} - \lambda_*\|_2^2] &= \mathbb{E}[\|\hat{\lambda} - \hat{\beta}\lambda_*\|_2^2 + \|(\hat{\beta} - 1)\lambda_*\|_2^2] \\
&= \mathbb{E}[\|\hat{\lambda} - \hat{\beta}\lambda_*\|_2^2] + \mathbb{E}[\|(\hat{\beta} - 1)\lambda_*\|_2^2] \\
&\lesssim \frac{2p^2}{\alpha_2}B_n + \mathbb{E}[(\hat{\beta} - 1)^2\|\lambda_*\|_2^2] \\
&\leq \frac{2p^2}{\alpha_2}B_n + \mathbb{E}[(\hat{\beta} - 1)^2] \\
&\lesssim \frac{2p^2}{\alpha_2}B_n + \frac{2p^3}{\alpha_2}B_n
\end{aligned}$$

as desired. □

Corollary 2 can be combined with Theorem 1 as follows. Suppose $\{\mu_i\}_{i=0}^p$ are a.c. measures supported on the open, convex, bounded set Ω satisfying **A1-A3**. Suppose these can be extended to the closure of Ω so that **A4-A6** hold; call these measures $\{\tilde{\mu}_i\}_{i=0}^p$. Note that the since $\tilde{\mu}_i, \mu_i$ are a.c. with densities that are equal a.e., the transport maps T_i between μ_0 and μ_i and the maps \tilde{T}_i between $\tilde{\mu}_0$ and $\tilde{\mu}_i$ satisfy $\mu_i(B) = \mu_0(\tilde{T}_i^{-1}(B))$, $\tilde{\mu}_i(B) = \tilde{\mu}_0(\tilde{T}_i^{-1}(B))$ for all Borel sets B . Thus, the Gram matrix of inner products between the displacement maps defined with the $\{\mu_i\}_{i=0}^p$ is the same as that defined with $\{\tilde{\mu}_i\}_{i=0}^p$. Hence, the optimal λ_* in Corollary 2 does indeed satisfy $\nu_{\lambda_*} = \mu_0$, that is, we get consistency towards coefficients realizing the optimal barycentric representation.

3 Covariance Estimation Experiment Details

3.1 Methods for Maximum Likelihood Estimation

In order to solve the maximum likelihood estimation problem we differentiate through a truncated version of [13] Algorithm 1 and perform projected gradient descent. This is implemented using the auto-differentiation library PyTorch. The procedure is summarized in Algorithm 3. Here $\text{SimplexProject}(x)$ is defined as

$$\text{SimplexProject}(x) = \arg \min_{y \in \Delta^p} \|x - y\|_2.$$

which enforces the constraints on λ at each iteration.

To compute $\nabla \mathcal{L}(\lambda)$ we use auto-differentiation to obtain a gradient of the procedure given in Algorithm 4. In this procedure the square root of a matrix is computed using SQIters number of Newton-Schulz iterations. The forward pass of the loss computation is given in Algorithm 4, and the gradient is obtained by back propagation through it.

Algorithm 3 MLE

Input: $\{S_i\}_{i=0}^p$, $\eta > 0$, $\text{MaxIters} > 0$, $\text{FPIters} > 0$, $\text{SQIters} > 0$
 $i \leftarrow 0, \lambda \leftarrow (1/p)\mathbf{1}$
while Not Converged and $i < \text{MaxIters}$ **do**
 $i \leftarrow i + 1$
 $\nabla \mathcal{L}(\lambda) \leftarrow \text{BackPropLoss}(\{S_j\}_{j=0}^p, \lambda, \text{FPIters}, \text{SQIters})$
 $\lambda \leftarrow \text{SimplexProject}(\lambda - \eta \nabla \mathcal{L}(\lambda))$
end while
Return λ

Algorithm 4 ComputeLoss

Input: $\{S_i\}_{i=0}^p$, λ , $\text{FPIters} > 0$, $\text{SQIters} > 0$
 $\text{BC} \leftarrow S_0$
for $j = 1, \dots, \text{FPIters}$ **do**
 $\text{BC_root} = \text{SquareRoot}(\text{BC}, \text{SQIters})$
 $\text{BC_root_inv} = \text{Invert}(\text{BC_root})$
 $\text{BC} = \text{BC_root_inv} \left(\sum_{i=1}^p \lambda_i \text{SquareRoot}(\text{BC_root}, \text{SQIters}, S_i \text{BC_root}) \right)$
 BC_root_inv
end for
Return $\text{Tr}(\text{BC}^{-1} S_0) + \log \det \text{BC}$

Parameter	Value
η	0.0003
MaxIters	500
FPIters	10
SQIters	10

Table 2: Parameters used when performing the maximum likelihood estimation.

The parameters that we chose in our experiments are given in Table 2. These parameters were sufficient to ensure that both the matrix square roots and fixed point iterations converged, and λ always converged before the final iteration was reached.

3.2 Considerations for Instability of MLE

Due to the requirement of differentiating through a matrix inverse in Algorithm 3 it is possible that the procedure may fail to numerically converge. In our trials, this happened in less than 0.5% of all attempts. When it does happen we discard the result, and these numerical failures impact neither the results of Figure 3, nor the timings of the trials.

4 MNIST Experiment Details

4.1 The MNIST Dataset

The MNIST Dataset [28] consists of a collection of 28×28 black and white images of hand-written digits. The brightness (or intensity) of each pixel is an integer between 0 and 255 with 0 being black and 255 being white.

Each image is initially a matrix $I^m \in \mathbb{R}_+^{28 \times 28}$, which is normalized to sum to one, $P_{ij}^m = I_{ij}^m / (\sum_{i',j'} I_{i',j'}^m)$ and then converted into a point cloud

$$\mu^m = \sum_{i,j=1}^{28} P_{ij}^m \delta_{(i,j)}.$$

4.2 White Noise Model

In order to apply additive noise we must generate white-noise images ζ . We generate ζ as a random matrix $\mathbb{R}^{28 \times 28}$ with each entry $\zeta_{ij} \sim \text{Unif}([0, 1])$. This random matrix is then converted into a point cloud using the same process as is used to turn the image matrix into a point cloud.

5 Document Classification Experiment Details

5.1 Datasets

Dataset	Description	B.O.W. Dim.	Avg. Words	\mathcal{C}
BBCSPORT	BBC sports articles labeled by sport	13243	117	5
20NEWS	canonical news article dataset	29671	72	20

Table 3: Dataset characteristics.

We show the characteristics of the datasets in Table 3. Bag of words dimension is the number of the unique words contained in each dataset. Average words is the average

number of the unique words in a document and \mathcal{C} is the number of classes of each of the datasets.

Both the BBCSport and News20 datasets that we used are those made publicly available from [24]. Both datasets consist of two components:

1. The datasets employ a word2vec [31] embedding to represent the words. Each word is represented as a point w on the unit sphere in \mathbb{R}^{300} and the semantic relationships between words are encoded in the geometry of the embeddings. Call the set of words \mathcal{W} , then the word2vec embedding is the matrix $W \in \mathbb{R}^{|\mathcal{W}| \times 300}$.
2. Each document D^m with label y^m is represented by a set of tuples $\{(c_i^m, \mathbf{w}_i^m)\}_{i=1}^n$, where n is the number unique words in D^m , c_i^m is the number of times \mathbf{w}_i^m shows in D^m .

We use the following procedure to convert a document into an empirical measure.

1. Given a document $D^m = \{(c_i^m, \mathbf{w}_i^m)\}_{i=1}^n$, let $\mathbf{p}^m \in \mathbb{R}^n$ be the probability vector with entries $p_i^m = c_i^m / (\sum_k c_k^m)$.
2. The document empirical measure is then

$$\mu^m = \sum_i p_i^m \delta_{\mathbf{w}_i^m}.$$

For convenience we filter out the points on which p^i places no support.

5.2 Procedure for Making Figure 5

As discussed in the main body, for $k \geq 2$ we select k documents from each topic and 100 test documents, and then repeat 50 times and average. In both plots in Figure 5 we iterate over different choices of k . To reduce computational load we reuse the test sets and reference documents within each trial across choices of k . For example the, all of the documents for $k = 4$ are used for $k \geq 5$. This allows the Wasserstein distances and estimates \hat{A}_{ij} to be cached avoiding further computation.

We note that this procedure produces plots in which each of the points individually has the same sampling pattern as if there was no re-use, it is only across samples that there is correlation. However, this correlation is shared across the prediction methods consider which preserves the fairness of the comparison of the methods.

6 Possible Rank Deficiency of \mathbf{A}

In general, there may exist a set $\Lambda \subset \Delta^p$ such that $|\Lambda| > 1$ and for all $\lambda \in \Lambda$ we have $\mu_0 = \nu_\lambda$. Indeed, suppose there are index sets I_1, I_2 such that $I_1 \cap I_2 = \emptyset$ and $I_1 \cup I_2 = \{1, 2, \dots, p\}$ but $\text{Bary}(\{\mu_i\}_{i \in I_1}) \cap \text{Bary}(\{\mu_i\}_{i \in I_2}) \neq \emptyset$. If $\mu_0 \in \text{Bary}(\{\mu_i\}_{i \in I_1}) \cap \text{Bary}(\{\mu_i\}_{i \in I_2})$ then it can be expressed as $\nu_{\lambda^1} \in \text{Bary}(\{\mu_i\}_{i \in I_1})$ and $\nu_{\lambda^2} \in \text{Bary}(\{\mu_i\}_{i \in I_2})$. Note that we may

interpret λ^1 and λ^2 as vectors in Δ^p with supports on I_1, I_2 , respectively. Now let $\alpha \in [0, 1]$ and let $\lambda = (1 - \alpha)\lambda^1 + \alpha\lambda^2$ (with the indices modified as needed). Then we have

$$\arg \min_{\nu \in \mathcal{P}_{2,ac}(\mathbb{R}^d)} \sum_{i=1}^p \frac{\lambda_i}{2} W_2^2(\nu, \mu_i) = \arg \min_{\nu \in \mathcal{P}_{2,ac}(\mathbb{R}^d)} (1-\alpha) \left(\sum_{i \in I_1} \frac{\lambda_i^1}{2} W_2^2(\nu, \mu_i) \right) + \alpha \left(\sum_{i \in I_2} \frac{\lambda_i^2}{2} W_2^2(\nu, \mu_i) \right) = \mu_0$$

where the last equality follows from the fact that if x minimizes both $f(x)$ and $g(x)$ then it must also minimize $\alpha f(x) + (1 - \alpha)g(x)$ for $\alpha \in [0, 1]$, and the assumption that μ_0 is the barycenter. This demonstrates that μ_0 actually corresponds to all $\lambda = \lambda = (1 - \alpha)\lambda^1 + \alpha\lambda^2$ for all $\alpha \in [0, 1]$.

Below, we will give a geometric characterization for the rank deficiency of A and how that relates to the optimality of the quadratic objective in Theorem 1. We first recall the quadratic problem over the probability simplex: $\min_{\lambda \in \Delta^p} \lambda^T A \lambda$. Since A is a symmetric and positive semidefinite matrix, a Rayleigh quotient analysis yields that the minimum possible value of the objective without simplex constraints is zero, which would be attained at an eigenvector corresponding to a zero eigenvalue. Given this fact, finding an exact solution to the above quadratic problem amounts to determining whether the probability simplex intersects the eigenspace of A associated with the zero eigenvalue. Hereafter, we will denote this space by E_0 .

Proposition 2. *If $E_0 \cap \Delta^p = \emptyset$, there is no $\lambda \in \Delta^p$ such that $\lambda^T A \lambda = 0$.*

Proof. Any $\lambda \in \Delta^p$ realizing $\lambda^T A \lambda = 0$ is an eigenvector corresponding to the zero eigenvalue. The result follows. \square

Proposition 2 shows in particular that exact minimization is only possible when $\text{rank}(A) < p$. Next, we state conditions under which there is a unique solution to the minimization program.

Proposition 3. *If $\text{rank}(A) = p - 1$ and $E_0 \cap \Delta^p \neq \emptyset$, then there is a unique $\lambda \in \Delta^p$ such that $\lambda^T A \lambda = 0$.*

Proof. If $\text{rank}(A) = p - 1$, $E_0 = \{\alpha v \mid \alpha \in \mathbb{R}\}$ for an eigenvector $v \neq \mathbf{0}$ corresponding to the zero eigenvalue. Let $\lambda \in E_0 \cap \Delta^p$. Then $\lambda = \alpha v$ for some $\alpha \in \mathbb{R}$. The constraint that $\lambda \in \Delta^p$ determines α uniquely, which gives the result. \square

Note that if E_0 non-trivially intersects the probability simplex and $\text{rank}(A) = p - 1$, the condition for uniqueness is equivalent to the statement that the origin can be written as a convex combination of the columns of A . We next consider the remaining case when $\text{rank}(A) < p - 1$; for simplicity of exposition, we focus on the specific case $\text{rank}(A) = p - 2$.

Proposition 4. *Let $\text{rank}(A) = p - 2$ and v_0 and v_1 be distinct eigenvectors corresponding to the zero eigenvalue of A . If $v_0 \in \Delta^p$ and $v_1 \in \Delta^p$, then there are infinitely many solutions to $\lambda^T A \lambda = 0$ with $\lambda \in \Delta^p$.*

Proof. By construction, $A v_0 = \mathbf{0}$ and $A v_1 = \mathbf{0}$. Let $\alpha \in [0, 1]$ and define $v_\alpha = \alpha v_0 + (1 - \alpha)v_1$. Since v_1 and v_2 are in Δ^p , it follows that $v_\alpha \in \Delta^p$. In addition, $A v_\alpha = \alpha A v_1 + (1 - \alpha)A v_2 = \mathbf{0}$ so that $v_\alpha \in E_0$. Since $\alpha \in [0, 1]$ was arbitrary, the result follows. \square

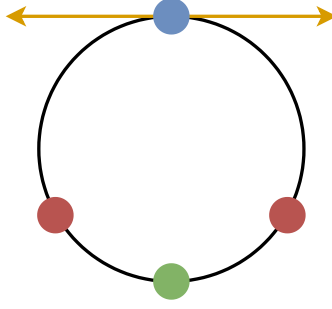


Figure 6: *Red*: The points z_1, z_2 . *Green*: The true barycenter x_λ . *Blue*: A Karcher mean which is not the barycenter. *Gold*: The tangent space at the blue point.

The main conclusion from the above Propositions is the following: if $\text{rank}(A) < p - 1$, the only way to mandate a unique solution is to require that only one eigenvector corresponding to the zero eigenvalue intersects with probability simplex. By convex geometry, if two eigenvectors corresponding to the zero eigenvalue intersect the probability simplex, there will be infinitely many solutions to the quadratic program.

7 Example of a Karcher Mean that is not a Barycenter

As mentioned in Section 2, special care must be made to ensure that any Karcher mean is also a barycenter. In this section we give a simple example which illustrates this point.

Consider $S^1 = \{x \in \mathbb{R}^2 : \|x\|_2 = 1\}$ with distance given by $\rho(x, y) = \cos^{-1}\langle x, y \rangle$. Let $z_1 \neq z_2 \in S^1$ with $z_1 \neq -z_2$, and $\lambda = (1/2, 1/2)$. Then the barycenter is given by

$$x_\lambda = \frac{z_1 + z_2}{\|z_1 + z_2\|_2}.$$

However, the point $-\frac{z_1 + z_2}{\|z_1 + z_2\|_2}$ is not the barycenter but it is a Karcher mean. This is illustrated in Figure 6. To show this rigorously one need only compute the Euclidean gradient and demonstrate that it is orthogonal to the tangent space.